

# Evaluation of Long-Term Cloud-Resolving Model Simulations Using Satellite Radiance Observations and Multifrequency Satellite Simulators

TOSHIHISA MATSUI AND XIPING ZENG

*Laboratory for Atmospheres, NASA Goddard Space Flight Center, Greenbelt, and Goddard Earth Science and Technology Center, University of Maryland, Baltimore County, Baltimore, Maryland*

WEI-KUO TAO

*Laboratory for Atmospheres, NASA Goddard Space Flight Center, Greenbelt, Maryland*

HIROHIKO MASUNAGA

*Hydrospheric Atmospheric Research Center, Nagoya University, Nagoya, Japan*

WILLIAM S. OLSON

*Laboratory for Atmospheres, NASA Goddard Space Flight Center, Greenbelt, and Joint Center for Earth Systems Technology, University of Maryland, Baltimore County, Baltimore, Maryland*

STEPHEN LANG

*Laboratory for Atmospheres, NASA Goddard Space Flight Center, Greenbelt, and Science Systems and Applications, Inc., Lanham, Maryland*

(Manuscript received 7 May 2008, in final form 24 November 2008)

## ABSTRACT

This paper proposes a methodology known as the Tropical Rainfall Measuring Mission (TRMM) Triple-Sensor Three-Step Evaluation Framework (T3EF) for the systematic evaluation of precipitating cloud types and microphysics in a cloud-resolving model (CRM). T3EF utilizes multisensor satellite simulators and novel statistics of multisensor radiance and backscattering signals observed from the TRMM satellite. Specifically, T3EF compares CRM and satellite observations in the form of combined probability distributions of precipitation radar (PR) reflectivity, polarization-corrected microwave brightness temperature ( $T_b$ ), and infrared  $T_b$  to evaluate the candidate CRM.

T3EF is used to evaluate the Goddard Cumulus Ensemble (GCE) model for cases involving the South China Sea Monsoon Experiment (SCSMEX) and the Kwajalein Experiment (KWAJEX). This evaluation reveals that the GCE properly captures the satellite-measured frequencies of different precipitating cloud types in the SCSMEX case but overestimates the frequencies of cumulus congestus in the KWAJEX case. Moreover, the GCE tends to simulate excessively large and abundant frozen condensates in deep precipitating clouds as inferred from the overestimated GCE-simulated radar reflectivities and microwave  $T_b$  depressions. Unveiling the detailed errors in the GCE's performance provides the better direction for model improvements.

## 1. Introduction

Cloud-resolving models (CRMs) explicitly resolve convective clouds and cloud systems on fine spatial and

temporal scales. CRMs with a one-moment bulk microphysics scheme explicitly predict the evolution of cloud dynamics associated with liquid and ice condensate masses and their associated latent heating and evaporative cooling in contrast to the implicit prediction in single-column schemes (SCMs); therefore, CRM simulations agree well with the observation in comparison with SCM simulations (Xu et al. 2002; Tao et al. 2003).

---

*Corresponding author address:* Toshihisa Matsui, Code 613.1, NASA Goddard Space Flight Center, Greenbelt, MD 20771.  
E-mail: toshihisa\_matsui-1@nasa.gov

With significant improvements in computational power over the last decade, CRM simulations can now be conducted for longer time periods in a 3D model configuration to obtain a better understanding of cloud and precipitation ensembles and radiative–convective equilibrium (Zeng et al. 2008; Zhou et al. 2007; Blossey et al. 2007; and many others). While they explicitly simulate cloud dynamics and microphysics evolution, CRMs are still subject to many uncertainties in cloud microphysical processes because of a lack of practical evaluation frameworks that can contrast CRM simulations with routine, extensive observations such as satellite measurements. Lang et al. (2007) recently initiated a more systematic approach to improving the microphysics in the Goddard Cumulus Ensemble model (GCE) based mainly on probability distributions from ground-based radar observations and limited satellite observations, but the two simulations used in the study were short-term and from a single location.

The Tropical Rainfall Measuring Mission (TRMM) satellite has operated continuously for over a decade, providing numerous, valuable observations of precipitating tropical cloud systems from its sensors: the Visible/Infrared Scanner (VIRS), the TRMM Microwave Imager (TMI), and the Precipitation Radar (PR; Kummerow et al. 1998). The retrieved rainfall rates are useful datasets for model evaluations (e.g., Zhou et al. 2007; Eitzen and Xu 2005), especially if the satellite-derived products are not based on model simulations. However, TRMM-derived physical products could contain their own biases due to uncertainties in the particle size spectra, particularly at the freezing level, in the retrieval algorithms (Kummerow et al. 2006). Therefore, it is often difficult to make a detailed evaluation of CRMs using TRMM-derived physical products because of differences in their estimation methods and microphysics assumptions. Thus, in order to evaluate CRMs more precisely against satellite observations, it is preferable to estimate satellite-consistent radiances from the model-generated microphysical distributions using radiative transfer calculations (i.e., satellite simulators) (Chaboureau et al. 2002; Chevallier and Bauer 2003; Masunaga et al. 2008), since direct satellite measurements (radiances) have much less uncertainty than retrieved physical parameters.

This paper introduces a practical CRM-evaluation framework using multisensor satellite simulators and fine-resolution radiance measurements from the TRMM satellite. The evaluation framework consists of (i) a CRM coupled with multisensor satellite simulators and (ii) a three-step statistical evaluation of brightness temperatures ( $T_b$ s) and radar reflectivities from the CRM simulations and TRMM observations. The approach is applied to long-term simulations from the GCE

for two cases: the South China Sea Monsoon Experiment (SCSMEX) and the Kwajalein Experiment (KWAJEX). These two cases are based on well-established field campaigns and have already been used previously for long-term CRM simulations to study tropical cloud and precipitation processes (Zeng et al. 2008; Zhou et al. 2007; Blossey et al. 2007). Those studies demonstrated that CRMs driven by the large-scale forcing could simulate the general features of the observed cloud processes but with essentially similar biases.

Zeng et al. (2008) found that the GCE tended to overestimate surface precipitation throughout the simulation periods for both SCSMEX and KWAJEX, and, as a result, column-integrated water vapor was largely underestimated compared to observations. They also found more convective cores with stronger updrafts in the 3D model configuration than in the 2D; therefore, regardless of the chosen microphysical parameterization, simulated precipitating cloud systems can be quite sensitive to differences in the dimensionality of the model. Zhou et al. (2007) found that GCE simulations for the SCSMEX case tended to produce a slightly larger convective to stratiform rain ratio than was estimated from the PR and TMI owing to less anvil (stratiform) cloud. They also found that underestimated high cloud fractions lead to an overestimation of outgoing longwave radiation in comparison with that estimated from the Clouds and the Earth's Radiant Energy System (CERES) sensors. Although using a different CRM and different observational data, Blossey et al. (2007) also found that their CRM also tended to underestimate high-cloud fraction, leading to an overestimate of the outgoing longwave radiation and an underestimate of the top-of-the-atmosphere (TOA) albedo during less rainy periods. These studies evaluated the CRM physical parameters as domain-averaged values.

In contrast to the previous studies, this paper focuses on a satellite radiance-based systematic evaluation of long-term CRM simulations by assessing the frequency of occurrence of different precipitation types as well as the microphysics of each precipitation type using multisensor satellite simulators. The paper is organized as follows. Section 2a details the configuration and setup of the long-term CRM simulations for the KWAJEX and SCSMEX cases. Section 2a describes the TRMM multisensor observations and the combinations used for evaluation. Section 2c describes the multisensor satellite simulators. Section 3 introduces a new satellite-based CRM evaluation framework. The framework is then used to evaluate the long-term CRM simulations in section 4. Section 5 discusses and summarizes issues related to the CRM simulations raised by the evaluation.

## 2. Numerical experiments and satellite measurements

### a. Cloud-resolving model simulations

In this study, long-term CRM simulations are performed using the GCE model (Tao 2003) for environments observed during the SCSMEX and KWAJEX field campaigns. The simulations are driven by surface turbulent fluxes, large-scale advective forcing for temperature and humidity, and horizontal wind tendencies derived from objective analysis, which statistically combines a variety of field measurements (Zhang et al. 2001). For a given high-quality long-term meteorological forcing, the GCE with imposed forcing provides a way to evaluate model configurations and physical processes (including the microphysics and cloud properties), if the simulated fields can be validated using independent observations. Two microphysics schemes are used in this study. One is the default Goddard microphysics scheme with three ice species (GM03; Tao 2003), and the other is a newly implemented microphysics scheme (GM07; Zeng et al. 2008; Lang et al. 2007). GM07 includes ice-nuclei concentrations for the Bergeron process (Zeng et al. 2008) and lowered collection efficiencies to reduce excessive amounts of graupel (Lang et al. 2007).

The grid configurations, dynamic core, and other physical parameterizations are identical except for the microphysics schemes (i.e., GM03 and GM07). The grid domain consists of  $256 \times 256 \times 41$  grid points in a Cartesian coordinate with a horizontal grid spacing of 1 km. The simulation domain is centered at  $9^\circ\text{N}$ ,  $167^\circ\text{E}$  for the KWAJEX case and at  $21^\circ\text{N}$ ,  $116^\circ\text{E}$  for the SCSMEX case. The time step is 6 s, and the simulation periods are from 24 July to 14 September 1999 for KWAJEX and from 6 May to 14 June 1998 for SCSMEX (Zeng et al. 2008).

Zeng et al. (2008) examined the sensitivity of simulated precipitation condensate to model dimensionality (i.e., 2D versus 3D grids) and microphysics (i.e., GM03 and GM07). Because precise and extensive measurements of water contents and drop size distributions (DSDs) of precipitation particles are limited even within a well-designed field campaign, in the present study these uncertain microphysical parameters are best evaluated through their impact on simulated multisensor radiance and backscattering signals in contrast to satellite observations (Chaboureau et al. 2002; Chevallier and Bauer 2003; Masunaga et al. 2008). Particularly, this method can evaluate the geophysical parameters through remotely sensed signals close to (or within) the deep convective core, where aircraft in situ measurements are nearly impossible.

### b. TRMM measurements

In this study, TRMM PR 13.8-GHz attenuation-corrected reflectivity from the TRMM 2A25 product, VIRS  $12\text{-}\mu\text{m}$  infrared brightness temperature ( $T_{b\text{IR}}$ ) from TRMM 1B01, and TMI 85.5-GHz dual-polarization microwave brightness temperature ( $T_{b85}$ ) from TRMM 1B11 (Kummerow et al. 1998) are used to evaluate the GCE simulations. PR reflectivity is sensitive to precipitating liquid and relatively large frozen condensates. VIRS  $T_{b\text{IR}}$  represents the cloud-top temperature above optically thick clouds. TMI  $T_{b85}$  depression (i.e., scattering) is correlated with the amount of relatively small precipitation-sized ice particles (Liu and Curry 1996). Observations from these three sensors were collected over the KWAJEX and SCSMEX sites during the GCE simulation periods. There are totals of 16 and 17 overpasses with enough scan coverage for the KWAJEX and SCSMEX sites, respectively. Significant PR reflectivity (above 17 dBZ) is also used to identify the radar echo-top height ( $H_{\text{ET}}$ ). Because the TMI sampled mixed land-ocean areas over the KWAJEX and SCSMEX sites, a polarization-corrected brightness temperature ( $PCT_{b85}$ ) is computed (Kidd 1998) in order to compensate for the inhomogeneity of surface emissivity via

$$PCT_{b85} = T_{b85V} + a(T_{b85V} + T_{b85H}),$$

where  $T_{b85V}$  and  $T_{b85H}$  are the  $T_b$  from the vertical and horizontal polarization channels at 85 GHz, respectively, and  $a = 0.8$ , which ensures that the inhomogeneity in surface emission is visually masked out over the two sites. VIRS  $T_{b\text{IR}}$  and TMI  $PCT_{b85}$  are collocated on the PR instantaneous field of view (IFOV). The PR and high-frequency TMI measurements have a fine IFOV of  $\sim 5$  km, close to the horizontal resolution of typical CRMs (i.e.,  $dx = dy = 1$  km in this study; thus a minimum resolvable dynamical spatial scale for the GCE simulations should be about 5 km). VIRS  $T_{b\text{IR}}$  measurements are convolved within the PR IFOV (i.e., 4.3 km at the surface) via a Gaussian beam pattern because of the smaller IFOV (i.e., 2.2 km at the surface) of the VIRS measurements (Masunaga and Kummerow 2005).

### c. Satellite simulators

The Goddard Satellite Data Simulation Unit (SDSU) is an end-to-end multisensor satellite simulator being built upon the original version developed at the Hydropheric Atmospheric Research Center (HyARC), Nagoya University, Japan (available online at <http://precip.hyarc.nagoya-u.ac.jp/sdsu/sdsu-main.html>). The Goddard SDSU simulates satellite-consistent radiances or backscattering from vertical profiles of model-simulated

atmospheric variables and condensates obtained from the Goddard Multi-Scale Modeling System with unified physics (Tao et al. 2008). At present, there are passive microwave, radar, passive visible–infrared, lidar, broadband shortwave and longwave, and International Satellite Cloud Climatology Project (ISCCP)-like simulators within the unified framework.

In this study, GCE-simulated atmospheric and condensate profiles are used to simulate TRMM PR-consistent reflectivity profiles via a radar simulator (Masunaga and Kummerow 2005), VIRS-consistent  $T_{bIR}$  through a spectrum infrared simulator [discrete ordinate radiative transfer (R-STAR); (Nakajima and Tanaka 1986; Stamnes et al. 1988)], and TMI-consistent  $T_{b85}$  through a passive microwave simulator [delta-Eddington two-stream radiative transfer with slant path view (Kummerow 1993; Olson and Kummerow 1996)]. All of the simulators are currently 1D and do not include 3D scattering effects. Within the simulators, the optical properties for condensates are derived via Mie theory (spherical assumption), while the DSD parameters for precipitation particles are specified in accordance with the GCE model (i.e., exponential size distributions with prescribed exponent-intercept parameters and bulk particle densities). The simulated  $T_{bS}$  and radar reflectivities are then convolved within the IFOV corresponding to each TRMM sensor through a Gaussian beam pattern similar to the TRMM observations (section 2b)<sup>1</sup> and sampled only at the actual TRMM orbiting time over the respective KWAJEX or SCSMEX sites. It should be noted that CRM-simulated non-precipitating cloud systems are not evaluated in this framework, and it is beyond the scope of this study.

### 3. TRMM Triple-Sensor Three-Step Evaluation Framework (T3EF)

Due to the inability of CRM simulations to accurately predict the location of precipitating cloud systems relative to the satellite observations, ensemble statistics of  $T_{bS}$  and radar reflectivities from the satellite observations and GCE simulations are compared. As a result, it is critical to identify subsets of the simulations and observations that represent similar cloud/precipitation systems. To this end, the TRMM Triple-Sensor Three-Step Evaluation Framework (T3EF), which systematically examines discrepancies between the model and observations by (i) creating joint diagrams of precipitating cloud types from collocated VIRS  $T_{bIR}$  and PR

$H_{ET}$  (Masunaga et al. 2005), (ii) constructing contoured frequency with altitude diagrams (CFADs) of PR reflectivity (Yuter and Houze 1995) for each precipitating cloud type, and (iii) constructing cumulative probability distributions of TMI  $PCT_{b85}$ , is introduced. Prior to actual evaluation of the CRM simulations, an observational sketch of T3EF is introduced to address the physical aspects of each radiance-based ensemble statistical evaluation.

#### a. Joint $T_{bIR}$ – $H_{ET}$ diagrams

Long-term simulations of the GCE model predict precipitating cloud ensembles over the same periods as TRMM-observed tropical precipitation systems. Different precipitating cloud systems are associated with different mesoscale processes and therefore differing amounts of latent heat release, evaporative cooling, and radiative heating (Tao et al. 2003; Olson et al. 2006). Consequently, it is critical to subcategorize and evaluate the frequencies of each of the different precipitating cloud systems (Masunaga and Kummerow 2006).

In this study, collocated VIRS  $T_{bIR}$  and PR  $H_{ET}$  are used to categorize tropical precipitation systems into four systems: shallow, congestus, midcold, and deep types, closely following the methods in Masunaga et al. (2005) with minor modifications. The shallow category ( $T_{bIR} > 260$  K and  $H_{ET} < 4$  km) encompasses shallow precipitating systems. The congestus category ( $T_{bIR} > 245$  K and  $4 \text{ km} < H_{ET} < 7$  km) generally represents cumulus congestus. The midcold category ( $T_{bIR} > 245$  K and  $4 \text{ km} < H_{ET} < 7$  km) represents a combination of cold cloud-top temperature and moderately high  $H_{ET}$  height, inferring stratiform systems with relatively small frozen condensate aloft. This category also encompasses cumulus congestus overlapped by the cirrus (anvil) clouds, as pointed out by Stephens and Wood (2007). The deep category ( $T_{bIR} < 260$  K and  $7 \text{ km} < H_{ET}$ ) represents deep convective systems and deep stratiform systems with relatively large frozen particles aloft (Fig. 1). For the purpose of model evaluation, this separation method is advantageous in that identical radiance-based separation methods can be applied to both the TRMM observations and simulator-coupled CRM simulations (Masunaga et al. 2008).

Figure 2 shows joint  $T_{bIR}$ – $H_{ET}$  diagrams from TRMM observations corresponding to the SCSMEX and KWAJEX cases. In the KWAJEX case, the TRMM observations show two distinct peaks in probability density ( $\sim 1.2\% \text{ km}^{-1} \text{ K}^{-1}$ ): in the shallow category with  $T_{bIR}$  near 285 K and  $H_{ET}$  near 3 km and in the deep category with  $T_{bIR}$  near 210 K and  $H_{ET}$  near 8 km. In the SCSMEX case, the TRMM observations show a strong peak in the deep category centered around 200 K

<sup>1</sup> This process convolved the GCE–SDSU simulated 1-km-grid radiance into 5-km IFOV.

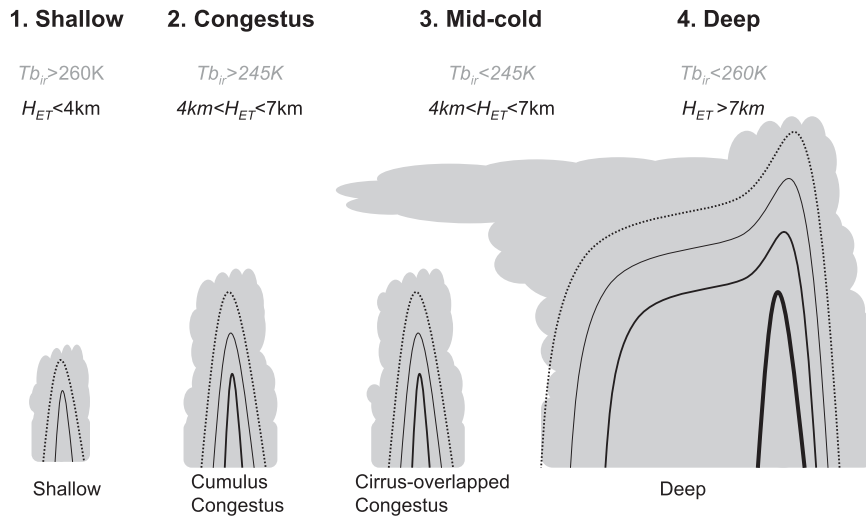


FIG. 1. Schematics of precipitating cloud types closely following the method in Masunaga et al. (2005) but slightly modified to account for the consideration in Stephens and Wood (2007). Gray shading represents cloud ice and liquid condensates, and contoured lines represent precipitation radar reflectivity (dotted lines represent the minimum detectable radar echo, while thicker solid lines represent larger echoes). Precipitation systems are categorized into 1) shallow, 2) congestus, 3) midcold, and 4) deep categories based upon infrared brightness temperature (closely related to cloud-top temperature) and precipitation radar echo-top height.

( $T_{b_{IR}}$ ) and 10 km ( $H_{ET}$ ) and another peak in the congestus category centered around 260 K ( $T_{b_{IR}}$ ) and 5 km ( $H_{ET}$ ). In contrast to the KWAJEX case (17.4% of shallow and 33.4% of deep categories), there are higher probability densities in the deep category (41.9%) and lower in the shallow category (11.5%). These results confirm that precipitation systems are much more organized and vigorous in the SCSMEX case than they are

in the KWAJEX case (Johnson et al. 2005; Yuter et al. 2005; Zeng et al. 2008). In addition, the probability densities for the midcold category (including stratiform and cirrus-overlapped congestus) in the SCSMEX case (23.3%) appear to be smaller than those in the KWAJEX case (31.8%). Johnson et al. (2005) reported that the stratiform rain fraction (26%) for convective systems from SCSMEX is smaller than that typical (40%) in the

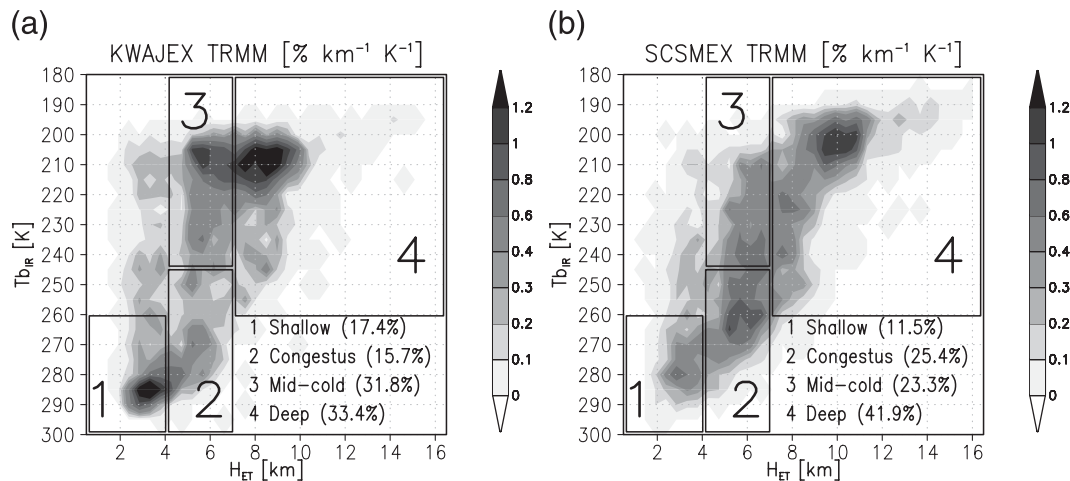


FIG. 2. Joint infrared brightness temperature ( $T_{b_{IR}}$ ) and radar echo-top height ( $H_{ET}$ ) diagrams based on TRMM observations for the (a) KWAJEX and (b) SCSMEX cases. Values represent the total probability densities for each precipitating cloud type (1: shallow, 2: congestus, 3: midcold, 4: deep).

tropics. Note that in the Fig. 2, the category with  $T_{bIR}$  less than 260 K and  $H_{ET}$  below 4 km is categorized as shallow precipitating clouds overlapped by the middle or high clouds (Masunaga et al. 2005). Because of the negligible population, this study does not examine this category.

### b. Type-classified reflectivity CFADs

CFADs are height-dependent probability density distributions of geophysical parameters (Yuter and Houze 1995). Thus, CFADs of PR reflectivities provide a useful statistical description that illustrates the effects of precipitation microphysics at different altitudes (Lang et al. 2007; Zhou et al. 2007; Blossey et al. 2007). Lumping the different precipitating cloud categories together in the analysis could, however, smear together the important microphysical characteristics associated with each precipitating cloud type (Lang et al. 2007; Blossey et al. 2007). For example, in the previous section, it was shown that SCSMEX has a higher probability of deep precipitating clouds. As such, grouping all of the cloud categories together would generate CFADs biased toward the characteristics of deep precipitating clouds. To avoid this kind of bias, reflectivity CFADs should be separately constructed for at least the convective and stratiform portions of precipitation systems (Yuter et al. 2005; Zhou et al. 2007). This study differentiates the CFADs into separate shallow, congestus, midcold, and deep categories as defined by the joint  $T_{bIR}$ - $H_{ET}$  diagrams (section 3a).

Figure 3 shows type-classified reflectivity CFADs for the KWAJEX and SCSMEX cases. Reflectivity CFADs were constructed by binning the reflectivities into 1-dBZ bins at each height increment (250 m). Shallow is the weakest category in terms of reflectivity intensity. Modal and maximum reflectivities are limited below 25 and 44 dBZ, respectively. Congestus (representing cumulus congestus) is a more vigorous category, with larger modal and maximum reflectivities than the shallow type. For shallow and cumulus congestus types, the reflectivity distribution broadens toward the surface, indicating the importance of coalescence and collection processes, which widen the raindrop spectra. CFADs for the midcold category appear to be relatively similar to those for the congestus category, but there is a subtle signal of bright band due to melting ice particles, especially in the SCSMEX case, at an altitude of about 5 km. However, these signals are weak at best, and greater melting signals appear in the deep category. The similarity of CFADs in midcold to those in congestus suggests that large amounts of cirrus (anvil)-overlapped cumulus congestus are categorized within the midcold derived by the joint  $T_{bIR}$ - $H_{ET}$  diagrams (Stephens and

Wood 2007). Below the 5-km altitude, the reflectivity distributions become relatively uniform with height in contrast to the shallow and cumulus congestus types, wherein the mode reflectivities gradually increased toward the surface.

The most remarkable CFADs are associated with the deep category. At high altitudes (i.e., above 10 km), reflectivities are narrowly distributed, and maximum values remain below  $\sim 30$  dBZ. These low PR reflectivities can be attributed to the presence of smaller nonspherical frozen precipitation particles. At middle altitudes (i.e., between 5 and 10 km), maximum reflectivities increase toward lower altitudes, which suggests a broadening and increase in particle sizes due to the aggregation and sedimentation of frozen particles. Modal reflectivity increases dramatically below 6 km because of the melting of frozen particles. At low altitudes (i.e., below 5 km), frozen condensates are almost completely melted, allowing liquid raindrops to dominate the radar backscattering signals. The high dielectric constant of liquid water results in larger reflectivities than at high altitudes. Reflectivity distributions below the melting layer are relatively uniform with height, particularly for the SCSMEX case, an indication that raindrop breakup and stochastic collection are combining to stabilize the raindrop size spectra. Compared to KWAJEX, the SCSMEX deep category has broader and larger reflectivities with higher echo-top height, all of which again confirm that the precipitation systems are much more vigorous in the SCSMEX case than they are in the KWAJEX case (Johnson et al. 2005; Yuter et al. 2005; Zeng et al. 2008).

### c. Type-classified cumulative probability distributions of $PCT_{b85}$

Although a passive microwave radiometer provides less specific information on the vertical profiles of condensates than the TRMM PR, the 85-GHz TMI channels are fairly sensitive to smaller-size frozen particles and ice water path in the upper portions of precipitating cloud systems (Yuter et al. 2005). At this frequency, precipitation-sized particles scatter the upwelling microwave radiation emission and thereby depress the outgoing microwave radiances at the TOA (Liu and Curry 1996). Therefore, to augment the reflectivity CFADs,  $T_b$ s from the TRMM satellite are assessed in terms of cumulative probability distributions of  $PCT_{b85}$  for the different precipitating cloud types. This evaluation is also important for the assessment of passive microwave sensor-based rainfall/latent heating retrieval algorithms, because the GCE simulations and simulated  $T_b$ s are used in the a priori databases of retrieval algorithms (Kummerow et al. 2006; Olson et al. 2006).

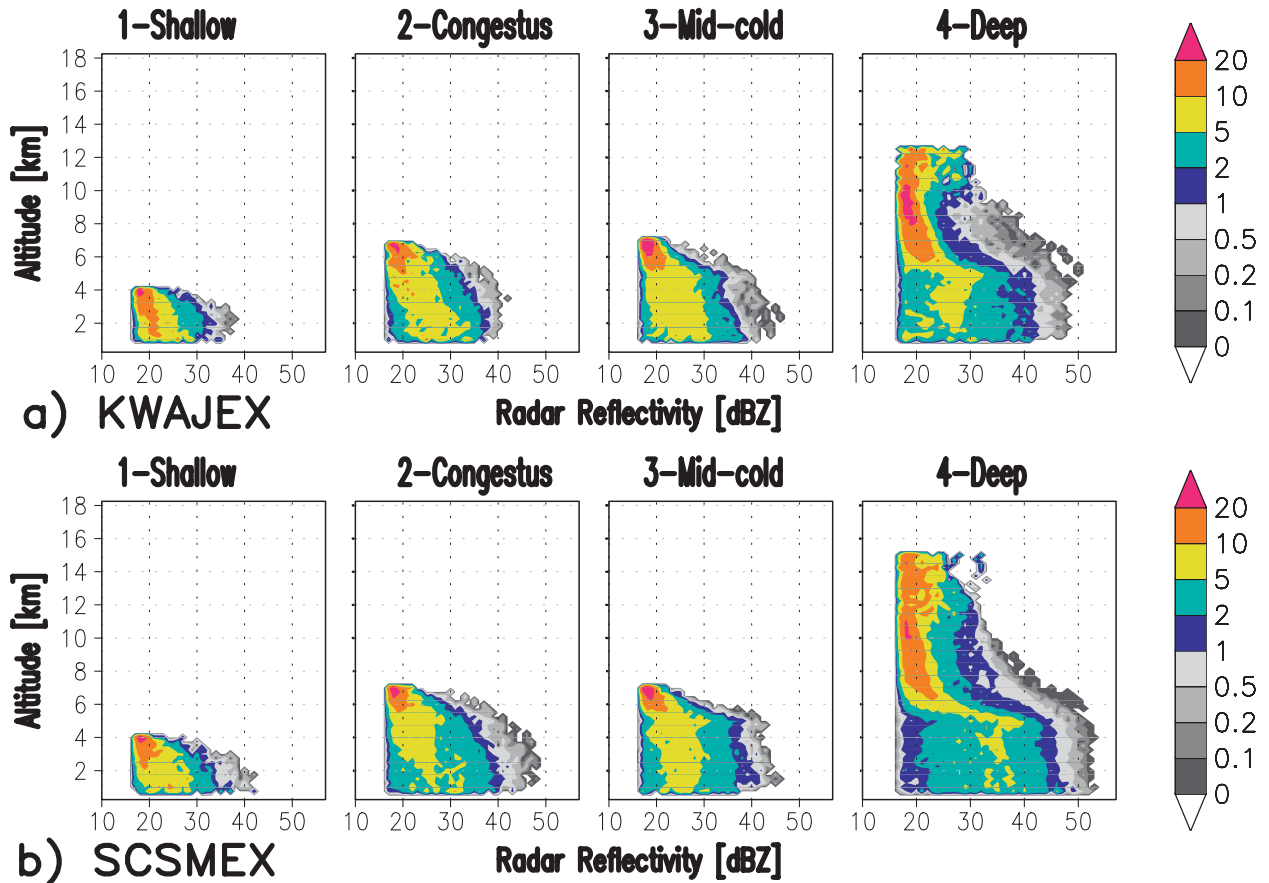


FIG. 3. Contoured frequency with altitude diagrams (CFADs) of precipitation radar reflectivity for the shallow, congestus, midcold, and deep categories for (a) KWAJEX and (b) SCSMEX.

Figure 4 shows cumulative probability distributions of  $PCT_{b85}$  (bin size is 10 K). It is quite discernible, particularly for the SCSMEX case, that the probability distributions trend toward lower  $PCT_{b85}$  values as the cloud types progress from the shallow to congestus to midcold to deep categories. This essentially means that the amount of frozen precipitation particles increases from shallow to deep precipitating clouds. It is worth noting that the probability distributions for the midcold category have larger  $PCT_{b85}$  depressions than do those for the congestus category, although the structures of their reflectivity CFADs appeared to be quite similar (Fig. 3). This is a manifestation of  $PCT_{b85}$  (85 GHz) depressions being highly sensitive to smaller-sized frozen precipitation particles, to which the PR (13.8 GHz) is relatively insensitive because of its longer wavelength. In contrast to SCSMEX, the probability distributions for the deep and midcold categories are nearly the same in KWAJEX, although the CFADs for these two types are dissimilar (Fig. 3). The KWAJEX  $PCT_{b85}$  depressions are also suppressed compared to those from SCSMEX, an indication that deep precipitating cloud is

more isolated and less vigorous in KWAJEX. These results highlight the utility of evaluating  $PCT_{b85}$  in addition to PR reflectivity.

#### 4. Evaluating the GCE simulations through T3EF

In this section, T3EF is used to evaluate the GCE simulations for KWAJEX and SCSMEX. It should again be noted that TRMM-consistent radiances are computed from the GCE simulations using multisensor satellite simulators, and those radiances are then contrasted against observed radiances in a three-step statistical evaluation.

##### a. Evaluation of precipitating cloud types by joint $T_{bIR}-H_{ET}$ diagrams

Joint  $T_{bIR}-H_{ET}$  diagrams are constructed from the GCE simulations for two different microphysics schemes (GM03 and GM07) using the visible-IR and radar simulators (Fig. 5). In the KWAJEX case, it is clear that both of the GCE experiments (i.e., GM03 and GM07) strongly overestimate the probability densities of the

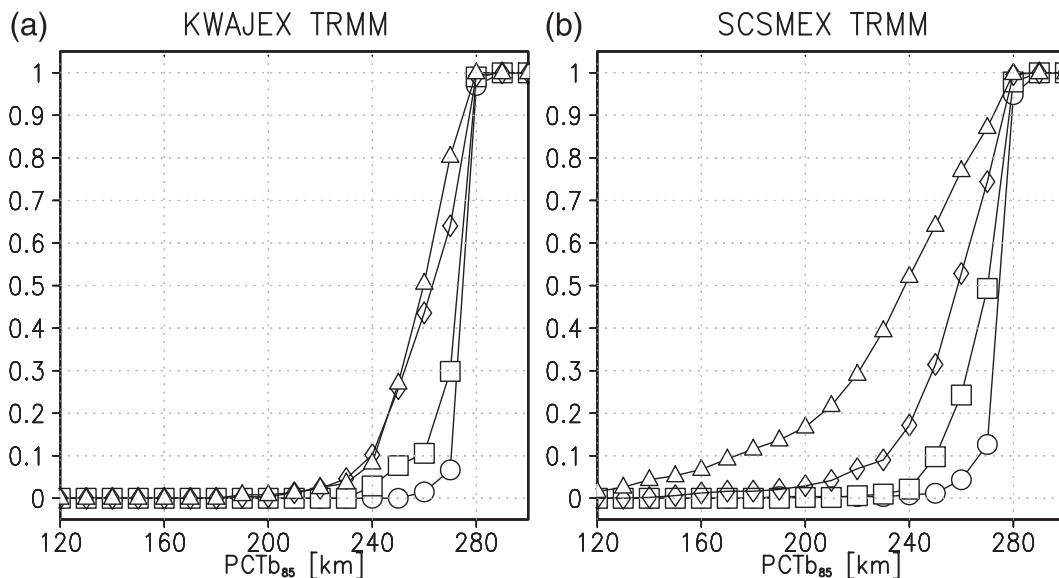


FIG. 4. Cumulative probability distributions of polarization-corrected TMI brightness temperature at 85 GHz ( $PCT_{b85}$ ; circles, shallow; squares, congestus; diamonds, midcold; and triangles, deep) for (a) KWAJEX and (b) SCSMEX.

shallow and congestus categories; the combined shallow and congestus probability densities are 71.7% for GM03 and 69.3% for GM07 compared with just 33.1% from the TRMM observations. On the other hand, combined probability densities of the deep and midcold categories (25.8% in GM03 and 28.8% in GM07) largely underestimate the TRMM observations (65.2%). GM07 performs slightly better in terms of the  $T_{bIR}$  ( $\approx$ cloud-top temperature) probability distributions for the deep and midcold categories compared to GM03. It should be noted that the probability densities for the deep category in the GCE simulations have a corrugated texture along the  $H_{ET}$  axis. This is an artifact of the current GCE (and almost all other CRMs) grid configurations that use a stretched vertical coordinate, which results in a coarser layer thickness ( $\sim 1$  km) than the PR resolution (0.25 km) in the middle/upper troposphere.

Overall, the GCE performs better in the SCSMEX environment than in the KWAJEX environment. The structure of the probability densities, particularly in GM03, is similar to that of the TRMM observations. Although the combined deep and midcold probability densities (71.5% for GM03 and 82.2% for GM07) slightly overestimate the TRMM observations (65.2%), the probability densities of the shallow category are very close (9.01%  $\sim$  11.5%). Unlike the KWAJEX case, GM03 performs slightly better than GM07. As noted earlier, there is a significant difference between the KWAJEX and SCSMEX cases that is attributable to differences in the environmental forcing and hence the

dynamics of the precipitation systems. The fact that the GCE performs better for SCSMEX is probably due to it having more organized precipitation systems driven by stronger large-scale forcing (Johnson et al. 2005), which are better resolved by the spatial grid spacing used in this study. The less vigorous KWAJEX case probably requires a finer spatial resolution to resolve the evolution of weaker, isolated, less-organized cumulus systems, as demonstrated by Lang et al. (2007). In addition, there is the possibility of forcing errors, discussed in section 5.

#### b. Evaluating precipitation microphysics by type-classified reflectivity CFADs

Instead of showing the entire probability distributions, the mean and maximum reflectivities are highlighted and compared between the TRMM observations and GCE simulations for the KWAJEX and SCSMEX cases. Although not shown here, the minimum reflectivity is always 17 dBZ (the minimum PR-detectable echo) for all cases (Fig. 6).

##### 1) SHALLOW

In both SCSMEX and KWAJEX, the mean reflectivity profiles of the TRMM observations gradually increase from 18 dBZ at the echo-top altitude to 25 dBZ near the surface; both the GM03 and GM07 profiles from the model agree quite well with these observations (within an accuracy of 2 dBZ). The maximum TRMM-observed reflectivities in KWAJEX are slightly smaller

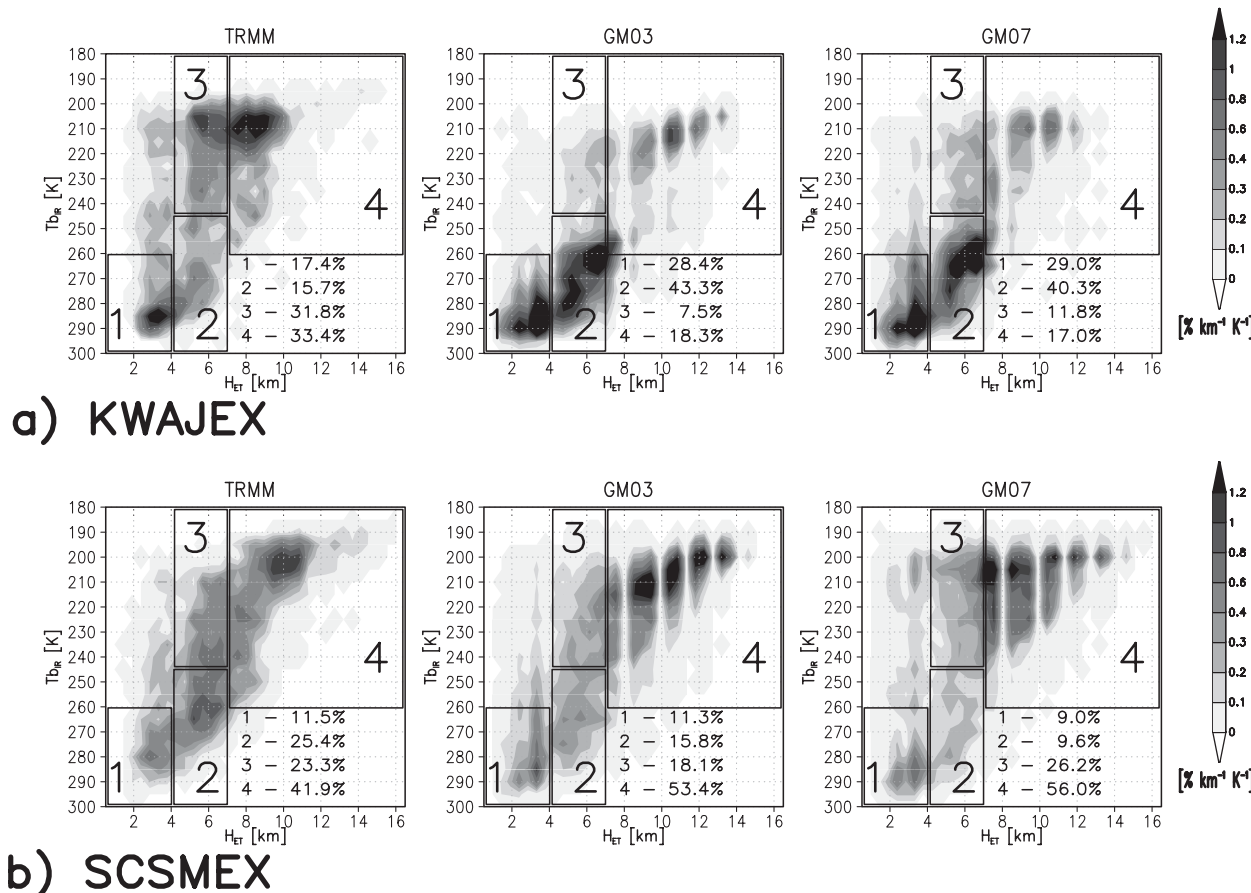


FIG. 5. Comparison of joint  $T_{bir}$ - $H_{ET}$  diagrams and probability densities for each precipitating cloud type between the TRMM observations and GCE simulations (GM03 and GM07) in (a) KWAJEX and (b) SCSMEX. Values as in Fig. 2.

(24–38 dBZ) than those in SCSMEX (27–42 dBZ) but again, both are well captured by GM03 and GM07.

2) CONGESTUS

Mean reflectivity profiles from the TRMM observations for both cases range from 18 dBZ at the echo-top altitude to 29 dBZ near the surface. While the GCE simulations slightly overestimate the TRMM mean reflectivities by about 3 dBZ, the most discernible discrepancy between the model and observations appears in the maximum reflectivity profiles for the KWAJEX case. The GCE simulations overestimate the maximum reflectivities by as much as 16 dBZ near the echo top and by 10 dBZ near the surface. The overestimated reflectivity in the upper layer is most likely due to the presence of high-density large frozen precipitation particles (see details in next section). For a given drop-size distribution and number concentration, a 16-dBZ bias is equivalent to a mean particle diameter in the GCE simulations that is nearly twice as large as that of the TRMM observations in the Rayleigh approxima-

tion. As parameterized in the GCE, the presence of large-sized particles will enhance the mean particle terminal velocity that suppresses deeper ice particles aloft. Thus, the presence of large ice-phase condensates could explain why the GCE overestimates the frequency of the congestus category while underestimating the frequency of the deep and midcold categories. But this argument does not go beyond the speculation level, and other potential sources of model biases are also discussed in the section 5. On the other hand, maximum reflectivities from the GCE simulations agree reasonably well with the TRMM observations for the SCSMEX case. Model deviations from the observed mean and maximum reflectivities are limited to 3 and 4 dBZ, respectively. In all cases, there is almost no difference in performance between GM03 and GM07.

3) MIDCOLD

GM03 and GM07 generally agree well with the TRMM observations in terms of the mean and maximum reflectivities, particularly in the KWAJEX case. In

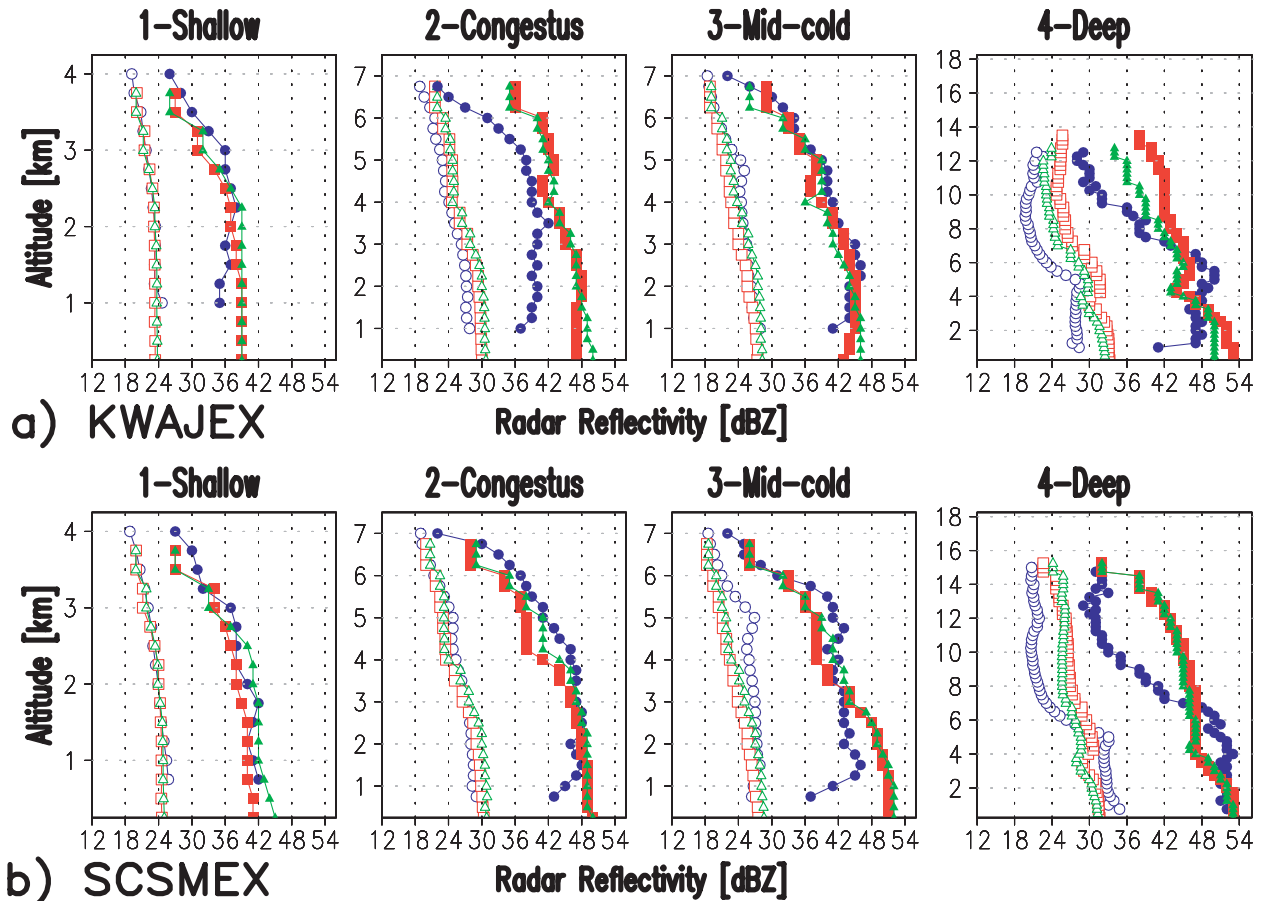


FIG. 6. Mean (open circles, TRMM; open squares, GM03; open triangles, GM07) and maximum (closed circles, TRMM; closed squares, GM03; closed triangles, GM07) reflectivity profiles from PR reflectivity CFADs for the (a) KWAJEX and (b) SCSMEX cases. Different vertical scales are used for each type of precipitating cloud.

the SCSMEX case, GM03 and GM07 tend to overestimate the maximum reflectivities by around 6 dBZ below an altitude of 4 km. Below an altitude of 1 km, the TRMM observations show a strong reduction in the maximum reflectivities, probably because of rain evaporation or surface clutter effect. None of the GCE simulations capture this feature. Again GM03 and GM07 do not have discernible differences in their reflectivity CFADs.

#### 4) DEEP

Among the four different cloud types, the largest discrepancies between the model and observations appear in the deep category. Although GM07 does perform somewhat better at higher altitudes in the KWAJEX case, the GCE simulations still generally do not capture the dramatic transitions in the reflectivity profiles observed by the TRMM satellite. At high altitudes, GM03 overestimates the mean and maximum reflectivities by as much as 5 and 12 dBZ, respectively, which sug-

gests that the GCE-simulated frozen precipitation particles are excessive both in size and amount. Near the melting layer ( $\sim 5$  km), both GM03 and GM07 underestimate the mean and maximum reflectivities by as much as 6 dBZ because of the lack of a melting signature in the simulations. Near the surface, both GM03 and GM07 agree well with the TRMM SCSMEX observations, but they tend to overestimate reflectivities for the KWAJEX case. As discussed in other previous modeling studies (Zhou et al. 2007; Blossey et al. 2007), the classified reflectivity CFADs highlight the uncertainties in the microphysics of simulated mixed-phase clouds.

#### c. Evaluating ice water paths by type-classified cumulative probability distributions of $PCT_{b85}$

Cumulative probability distributions of  $PCT_{b85}$  were constructed from  $T_{b85}$  values calculated from the GCE simulations for the KWAJEX and SCSMEX cases (Fig. 7). To better understand this statistical evaluation,

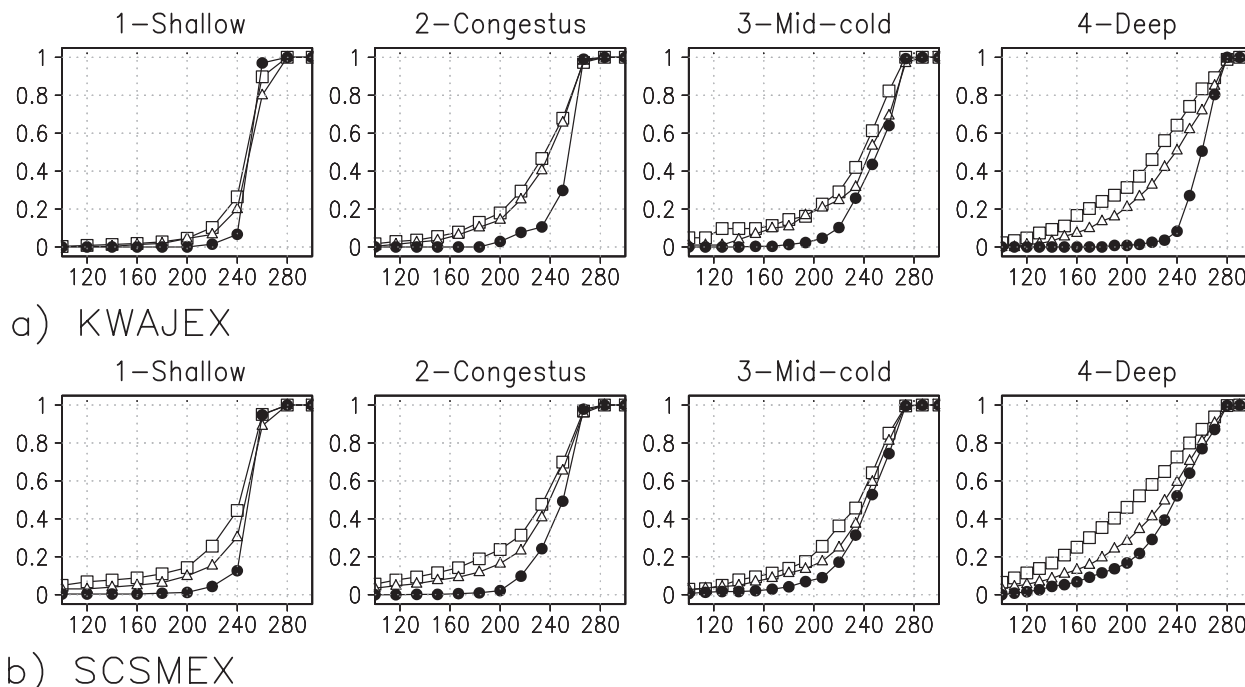


FIG. 7. Cumulative probability distributions of polarization-corrected TMI brightness temperature at 85 GHz ( $PCT_{b85}$ ; closed circles, TRMM; open squares, GM03; open triangles, GM07) for the shallow, congestus, midcold, and deep categories for (a) KWAJEX and (b) SCSMEX.

condensates from the GCE simulations are vertically integrated over the same sampling periods for the shallow, congestus, midcold, and deep categories (Table 1).

### 1) SHALLOW

Because of the absence of appreciable amounts of ice particles in this category (Table 1), cumulative probability distributions of shallow clouds can be characterized by the following parameters: background  $T_b$ , radiance emission from clouds, scattering of microwave radiance due to raindrops, and scattering of ice water path from overlapped neighboring pixels. Errors in the background  $PCT_{b85}$  are very small, because the GCE simulations are forced by an observation-assimilated variational analysis (Zhang et al. 2001). The emission of microwave radiance from clouds is also a small contribution (Liu and Curry 1996). The amount of rain is also very small (Table 1). Thus, discrepancies between the model and observations in the probability distributions most likely represent noise from neighboring pixels. Because the conical-tracking view of precipitation systems from the TMI channels ( $52.8^\circ$  viewing angle) is collocated with the cross-tracking view from the VIRS and PR sensors ( $-17^\circ \sim +17^\circ$ ), so is the combination of GCE-SDSU simulated radiances. In particular, the GCE simulations for the SCSMEX case tend to have unrealistically large depressions of  $PCT_{b85}$  for the shallow

type. Precipitation systems in SCSMEX are so organized that shallow precipitation types are frequently accompanied by deep precipitating clouds. In addition, because of the cyclic boundary conditions used in the GCE simulations, precipitation systems with fast propagation speeds tend to be densely populated within the simulation domain. These factors increase the likelihood of deep clouds overlapping shallow ones along the slant view of the TMI sensor and  $PCT_{b85}$ .

### 2) CONGESTUS

The GCE simulations tend to overestimate  $PCT_{b85}$  depressions for both KWAJEX and SCSMEX. These depressions can also be attributed to noise from neighboring pixels, but for midcold, the GCE simulates appreciable amounts of snow and graupel that can increase  $PCT_{b85}$  depressions (Table 1). This is unlikely to be observed in real cumulus congestus as they commonly do not glaciate (Johnson et al. 1999). The GM07 simulations produce less graupel than the GM03 while increasing the combined amount of liquid cloud, rain, and snow (Table 1). Because graupel is defined to be a higher-density frozen particle in the GCE model and also in the passive microwave simulator, it has a greater single-scattering albedo for a given ice water content. As a result, the  $PCT_{b85}$  depressions in GM03 are slightly reduced in GM07. The GCE simulations for KWAJEX

TABLE 1. Mean vertically integrated condensates ( $\text{kg m}^{-2}$ ) for the shallow, congestus, midcold, and deep categories.

	Shallow		Congestus		Midcold		Deep	
	GM03	GM07	GM03	GM07	GM03	GM07	GM03	GM07
<b>KWAJEX</b>								
Cloud	0.16	0.16	0.35	0.37	0.03	0.27	0.24	0.31
Rain	0.12	0.12	0.70	0.78	0.18	0.46	1.39	1.33
Cloud ice	0.00	0.00	0.00	0.00	0.06	0.19	0.37	0.47
Snow	0.01	0.01	0.05	0.10	0.09	0.17	0.15	0.43
Graupel	0.01	0.00	0.31	0.23	0.24	0.19	2.32	1.42
<b>SCSMEX</b>								
Cloud	0.27	0.30	0.39	0.42	0.18	0.23	0.25	0.24
Rain	0.15	0.15	0.64	0.78	0.41	0.47	1.03	0.95
Cloud ice	0.00	0.00	0.00	0.00	0.07	0.28	0.65	0.88
Snow	0.01	0.01	0.04	0.08	0.12	0.25	0.22	0.82
Graupel	0.01	0.00	0.18	0.13	0.29	0.14	2.70	1.67

generate nearly twice as much graupel than those for SCSMEX. This could explain the overestimation of maximum radar reflectivity near echo top in the cumulus congestus for the KWAJEX simulations (Fig. 6).

### 3) MIDCOLD

The GCE simulations slightly overestimate but, in general, reasonably capture the observed probability distributions in the SCSMEX case. Probably because of the relatively low amount of graupel ( $0.14 \text{ kg m}^{-2}$ ; Table 1), the  $PCT_{b85}$  depressions in GM07 are suppressed in comparison with GM03. In conjunction with the reflectivity CFAD analysis, it appears that the GCE SCSMEX simulations fairly well predict the precipitation-sized ice water path in this particular environment, which would lend more confidence to the passive-microwave retrieval algorithms in this type of precipitation system (Kummerow et al. 2006; Olson et al. 2006). Similarly, GM07 performs better than GM03 for the KWAJEX case; however, both simulations overpredict  $PCT_{b85}$  depressions, implying that the GCE simulations contain too much precipitation-sized ice (graupel and snow).

### 4) DEEP

Similar to the midcold type, the GCE overpredicts the  $PCT_{b85}$  depressions, probably owing to excessive amounts of frozen precipitation particles. For both the KWAJEX and SCSMEX cases, GM07 performs better than GM03, because GM07 tends to reduce the amount of high-density frozen condensate (graupel) in the deep category by as much as 40% (Table 1). These results suggest that simulated  $T_{b85}$  from the GCE is biased toward lower values for the deep category. Together with the reflectivity CFAD analysis (section 4b), it appears that the GCE generates too much frozen precipitation in the deep category for both the KWAJEX and

SCSMEX cases. Note that large frozen particle amounts translate into larger particle sizes in the exponential drop-size distributions with their fixed intercept. Therefore, excessive amounts of simulated frozen particles could exacerbate the model biases in the reflectivity CFADs and  $PCT_{b85}$  probability distributions. In comparison with the SCSMEX case, observed depressions of  $PCT_{b85}$  are rather small in the KWAJEX case. Nevertheless, GCE simulations cannot capture the observed regional difference in  $PCT_{b85}$  distributions.

## 5. Summary and discussion

Long-term simulations of convective cloud systems observed during SCSMEX and KWAJEX using the GCE model are evaluated through comparison between TRMM observations and simulated radiances and reflectivities using multisensor simulators. A proposed methodology for evaluating the simulated radiances and reflectivities using three of TRMM's sensors, known as T3EF, was used to systematically evaluate the performance of the GCE. While the GCE simulations are in reasonable agreement with the TRMM measurements in some aspects, major simulation biases found in this study include the following:

- a tendency for the GCE to overestimate the frequency of congestus and underestimate the occurrence of the deep and midcold categories for the KWAJEX case, and
- a tendency for the GCE to produce excessive amounts and therefore sizes of frozen condensate in the congestus and deep categories for both the KWAJEX and SCSMEX cases.

These biases appear to be common features in long-term 3D CRM simulations with one-moment bulk microphysics (Zeng et al. 2008; Zhou et al. 2007; Blossey

et al. 2007) and could be related to the following three issues:

- (i) Large-scale forcing. The long-term GCE simulations were driven by meteorological forcing obtained from variational analysis (Zhang et al. 2001). This analysis blended all possible observations to obtain the best estimates of area-averaged variables for the analysis domain over the KWAJEX and SCSMEX sites. Unlike KWAJEX, the precipitation systems in SCSMEX are dominated by mesoscale convective systems (MCSs) driven by stronger large-scale environmental forcing (Johnson et al. 2005). Thus, it may be more realistic to drive the GCE with area-averaged (approximately hundreds of kilometers) forcing from SCSMEX than from KWAJEX. On the other hand, the vertical resolution of meteorological forcing should be even finer for simulating relatively weak precipitation systems, such as in the KWAJEX case.
- (ii) Grid configurations. In addition to the scale of the meteorological forcing, a finer spatial resolution in the GCE may be needed to better simulate the less-organized precipitation systems in the KWAJEX case. For example, Lang et al. (2007) found that GCE simulations using 1-km grid spacing tended to form deep convection abruptly, while 250-m grid spacing realistically simulated the gradual transition from shallow to deep convection that was observed during the TRMM Large-Scale Biosphere–Atmosphere Experiment in Amazonia (TRMM LBA). However, at present, it is impractical to conduct long-term CRM simulations with 250-m grid spacing. This would require a lot more (~50 times) computing time.
- (iii) Ice microphysics. Besides the issues related to large-scale forcing and grid configurations, the GCE simulates overly large radar reflectivities in the upper troposphere and overly strong microwave  $T_b$  depressions. All of these results suggest that the one-moment bulk microphysics tends to simulate excessively large amounts and sizes of precipitation ice. The new Goddard microphysics scheme (GM07) results in some improvement in terms of microwave  $T_b$ s by reducing the amount of graupel; however, it worsened the already poor estimation of shallow and cumulus congestus frequencies in the SCSMEX case. The ice microphysics issues have been discussed in previous modeling studies (e.g., Lang et al. 2007; Zeng et al. 2008; Zhou et al. 2007; Blossey et al. 2007). The overly large-sized precipitation ice simulated by the model could enhance the terminal velocity and thus the precipi-

tation efficiency, suppressing deeper convection in the KWAJEX case. This could be the reason that the GCE simulations generate too many cumulus congestus and too few midcold and deep precipitating-cloud types in the KWAJEX case. Although this idea does not go beyond the speculation level, Blossey et al. (2007) proposed a similar hypothesis from their long-term simulations for KWAJEX.

Technically, these three modeling deficiencies are commonly discussed to different degrees in previous work (e.g., Lang et al. 2007; Zeng et al. 2008; Zhou et al. 2007; Blossey et al. 2007; Eitzen and Xu 2005), and complete resolution of these deficiencies is not attempted in this manuscript. Nevertheless, the intention of this paper is to introduce a new practical CRM evaluation framework, the so-called TRMM Triple-Sensor Three-Step Evaluation Framework (T3EF).

Instead of using the in situ (or aircraft)-observed geophysical parameters, the new framework (T3EF) uses multisensor satellite simulators and direct radiance observation from the TRMM satellite. T3EF revealed detailed errors in the CRM's performance that could not be assessed by surface precipitation analysis only. Of course, although it is limited in time and space, the in situ (aircraft or ground-based sampling) observation during field campaigns is also a valuable framework for evaluating/improving CRM performances (Xu et al. 2002; Luo et al. 2008). In addition to traditional field campaigns, satellite-based evaluation techniques will be most valuable for evaluating and improving model performance over the satellite-overpassing area and periods. The multisensor simulator-based evaluation approach can reduce the uncertainties and discrepancies in assumption between CRMs and satellite retrieval algorithms (Chaboureau et al. 2002; Chevallier and Bauer 2003; Masunaga et al. 2008).

T3EF is a TRMM stand-alone framework that can evaluate CRMs over most of the tropics, including over land and ocean through day and night. Therefore, with accurate global reanalysis, a satellite-radiance-based CRM intercomparison study over different tropical environments can be proposed in the near future following the method in Eitzen and Xu (2005), in order to test/improve 3D CRM simulations with a more complex microphysics scheme at different model grid spacings.

*Acknowledgments.* This research was supported by the NASA Headquarters Atmospheric Dynamics and Thermodynamics Program and the NASA Tropical Rainfall Measuring Mission (TRMM). The authors are grateful to Dr. R. Kakar at NASA HQ for his support of this research. This program was also supported by the

NASA MAP program. The authors are grateful to Dr. D. Anderson at NASA HQ. The authors also acknowledge NASA GSFC and Ames Research Center for computer time used in this research, and thank Wesley Berg and two anonymous reviewers and an editor for their constructive comments and suggestions.

## REFERENCES

- Blossey, P. N., C. S. Bretherton, J. Cetrone, and M. Kharoutdinov, 2007: Cloud-resolving model simulations of KWAJEX: Model sensitivities and comparisons with satellite and radar observations. *J. Atmos. Sci.*, **64**, 1488–1508.
- Chaboureaud, J.-P., J.-P. Cammas, P. J. Mascart, J.-P. Pinty, and J.-P. Lafore, 2002: Mesoscale model cloud scheme assessment using satellite observations. *J. Geophys. Res.*, **107**, 4301, doi:10.1029/2001JD000714.
- Chevallier, F., and P. Bauer, 2003: Model rain and clouds over oceans: Comparison with SSM/I observations. *Mon. Wea. Rev.*, **131**, 1240–1255.
- Eitzen, Z. A., and K.-M. Xu, 2005: A statistical comparison of deep convective cloud objects observed by an Earth Observing System satellite and simulated by a cloud-resolving model. *J. Geophys. Res.*, **110**, D15S14, doi:10.1029/2004JD005086.
- Johnson, R. H., T. M. Rickenbach, S. A. Rutledge, P. E. Ciesielski, and W. H. Schubert, 1999: Trimodal characteristics of tropical convection. *J. Climate*, **12**, 2397–2418.
- , S. L. Aves, P. E. Ciesielski, and T. D. Keenan, 2005: Organization of oceanic convection during the onset of the 1998 East Asian Summer Monsoon. *Mon. Wea. Rev.*, **133**, 131–148.
- Kidd, C., 1998: On rainfall retrieval using polarization-corrected temperatures. *Int. J. Remote Sens.*, **19**, 981–996.
- Kummerow, C., 1993: On the accuracy of the Eddington approximation for radiative transfer in the microwave frequencies. *J. Geophys. Res.*, **98**, 2757–2765.
- , W. Barnes, T. Kozu, J. Shiue, and J. Simpson, 1998: The Tropical Rainfall Measuring Mission (TRMM) sensor package. *J. Atmos. Oceanic Technol.*, **15**, 809–817.
- , W. Berg, J. Thomas-Stahle, and H. Masunaga, 2006: Quantifying global uncertainties in a simple microwave rainfall algorithm. *J. Atmos. Oceanic Technol.*, **23**, 23–37.
- Lang, S., W. K. Tao, J. Simpson, R. Cifelli, S. Rutledge, W. Olson, and J. Halverson, 2007: Improving simulations of convective systems from TRMM LBA: Easterly and westerly regimes. *J. Atmos. Sci.*, **64**, 1141–1164.
- Liu, G., and A. Curry, 1996: Large-scale cloud features during January 1993 in the North Atlantic Ocean as determined from SSM/I and SSM/T2 observations. *J. Geophys. Res.*, **101**, 7019–7032.
- Luo, Y., K. M. Xu, H. Morrison, and G. McFarquhar, 2008: Arctic mixed-phase clouds simulated by a cloud-resolving model: Comparison with ARM observations and sensitivity to microphysics parameterizations. *J. Atmos. Sci.*, **65**, 1285–1303.
- Masunaga, H., and C. D. Kummerow, 2005: Combined radar and radiometer analysis of precipitation profiles for a parametric retrieval algorithm. *J. Atmos. Oceanic Technol.*, **22**, 909–929.
- , and —, 2006: Observations of tropical precipitating clouds ranging from shallow to deep convective systems. *Geophys. Res. Lett.*, **33**, L16805, doi:10.1029/2006GL026547.
- , T. S. L'Ecuyer, and C. D. Kummerow, 2005: Variability in the characteristics of precipitation systems in the tropical Pacific. Part I: Spatial structure. *J. Climate*, **18**, 823–840.
- , M. Satoh, and H. Miura, 2008: A joint satellite and global cloud-resolving model analysis of a Madden-Julian Oscillation event: Model Diagnosis. *J. Geophys. Res.*, **113**, D17210, doi:10.1029/2008JD009986.
- Nakajima, T., and M. Tanaka, 1986: Matrix formulations for the transfer of solar radiation in a plane-parallel scattering atmosphere. *J. Quant. Spectrosc. Radiat. Transfer*, **35**, 13–21.
- Olson, W. S., and C. D. Kummerow, 1996: Simulated retrieval of precipitation profiles from TRMM Microwave Imager and precipitation radar data. Preprints, *Eighth Conf. on Satellite Meteorology and Oceanography*, Atlanta, GA, Amer. Meteor. Soc., 248–251.
- , and Coauthors, 2006: Precipitation and latent heating distributions from satellite passive microwave radiometry. Part I: Improved method and uncertainties. *J. Appl. Meteor. Climatol.*, **45**, 702–720.
- Stammes, K. H., S.-C. Tsay, W. Wiscombe, and K. Jayaweera, 1988: Numerically stable algorithm for discrete-ordinate-method radiative transfer in multiple scattering and emitting layered media. *Appl. Opt.*, **27**, 2502–2509.
- Stephens, G. L., and N. B. Wood, 2007: Properties of tropical convection observed by millimeter-wave radar systems. *Mon. Wea. Rev.*, **135**, 821–842.
- Tao, W. K., 2003: Goddard Cumulus Ensemble (GCE) Model: Application for understanding precipitation processes. *Cloud Systems, Hurricanes and the Tropical Rainfall Measuring Mission (TRMM): A Tribute to Dr. Joanne Simpson*, Meteor. Monogr., No. 51, Amer. Meteor. Soc., 103–138.
- , D. Starr, A. Hou, P. Newman, and Y. Sud, 2003: A cumulus parameterization workshop. *Bull. Amer. Meteor. Soc.*, **84**, 1055–1062.
- , and Coauthors, 2008: Goddard multi-scale modeling systems with unified physics. *GEWEX Newsletter*, Vol. 18, No. 1, International GEWEX Project Office, Silver Spring, MD, 6–9.
- Xu, K.-M., and Coauthors, 2002: An intercomparison of cloud-resolving models with the atmospheric radiation measurement summer 1997 intensive observation period data. *Quart. J. Roy. Meteor. Soc.*, **128**, 593–624.
- Yuter, S. E., and R. A. Houze Jr., 1995: Three-dimensional kinematic and microphysical evolution of Florida cumulonimbus. Part II: Frequency distributions of vertical velocity, reflectivity, and differential reflectivity. *Mon. Wea. Rev.*, **123**, 1941–1963.
- , —, E. A. Smith, T. T. Wilheit, and E. Zipser, 2005: Physical characterization of tropical oceanic convection observed in KWAJEX. *J. Appl. Meteor.*, **44**, 385–415.
- Zeng, X., W. K. Tao, S. Lang, A. Y. Hou, M. Zhang, and J. Simpson, 2008: On the sensitivity of atmospheric ensemble states to cloud microphysics in long-term cloud-resolving model simulations. *J. Meteor. Soc. Japan*, **86A**, 45–65.
- Zhang, M. H., J. L. Lin, R. T. Cederwall, J. J. Yio, and S. C. Xie, 2001: Objective analysis of ARM IOP data: Method and sensitivity. *Mon. Wea. Rev.*, **129**, 295–311.
- Zhou, Y. P., and Coauthors, 2007: Use of high-resolution satellite observations to evaluate cloud and precipitation statistics from cloud-resolving model simulations. Part I: South China Sea Monsoon experiment. *J. Atmos. Sci.*, **64**, 4309–4329.